# Elementary seismological analysis applied to the April 6, 2009 L'Aquila mainshock and its larger aftershock

F. Di Luccio[1] and N.A. Pino[2]

[1] *Istituto Nazionale di Geofisica e Vulcanologia, Sismologia e Tettonofisica, Roma, Italy*

[2] *Istituto Nazionale di Geofisica e Vulcanologia, Osservatorio Vesuviano, Napoli, Italy*

**ABSTRACT**   To understand the source complexity of the April 6, 2009 L'Aquila earthquake ($M_W$ = 6.3), a quick seismological analysis is done on the waveforms of the mainshock and the larger aftershock that occurred on April 7, 2009. We prove that a simple waveform analysis gives useful insights into the source complexity, as soon as the seismograms are available after the earthquake occurrence, whereas the reconstruction of the rupture dynamics through the application of sophisticated techniques requires a definitely longer time. We analyzed the seismograms recorded at broadband and strong motion stations and provided firm constraints on rupture kinematics, slip distribution, and static surface deformation, also discriminating the actual fault plane. We found that two distinct rupture patches associated with different fracture propagation directions and possibly occurring on distinct rupture planes, characterized the source kinematics of the April 6 events. An initial updip propagation successively proceeds toward SE, possibly on a different plane. We also show that the same processing, applied to the April 7, 2009 aftershock ($M_W$ = 5.6), allows us to obtain useful information also in the case of lower magnitude events. Smaller events with similar location and source mechanism as the mainshock, to be used as Green's empirical function, occur in the days before or within tens of minutes to a few hours after the mainshock. These quick, preliminary analyses can provide useful constraints for more refined studies, such as inversion of data for imaging the rupture evolution and the slip distribution on the fault plane. We suggest implementing these analyses for real, automatic or semi-automatic, investigations.

**Key words:** 2009 L'Aquila earthquake, seismic source, seismogram analysis.

## 1. Introduction

As experienced in the past (1997–1998 Umbria-Marche, central Italy, $M_{Lmax}$=5.8; 2002 Molise, southern Italy, $M_L$ = 5.4), an intermediate magnitude, highly destructive, earthquake hit central Italy, causing about 300 victims and severe damage in the city of L'Aquila and its surroundings. The mainshock, with an $M_W$ = 6.3 and a significantly different $M_L$ = 5.8, occured at a depth of 9 km and its focal mechanism was a pure normal fault (Pondrelli *et al.*, 2010). On April 7, at 17:47 UTC, a strong aftershock ($M_W$ = 5.6, $M_L$ = 5.3) occurred at 14 km depth, about 15 km SE of the mainshock and its focal mechanism was a normal fault with a consistent strike-

slip component (Pondrelli *et al.*, 2010).

The L'Aquila sequence is located in the Apennines, where most of the Italian destructive earthquakes (*M* > 6) struck in the past. The area is the result of a superimposition of the Quaternary extensional tectonics onto the Neogene compressive one. The compressional orogenic tectonics (Patacca *et al.*, 1992) produced the progressive NE migration of the Apenninic arc related to the flexural retreat of the lithospheric plate located in the Adriatic Sea (Doglioni, 1991). While compressive structures (over-thrusts) affected the progressive migration of the Apenninic front, with contemporaneous rifting processes occurring in the Tyrrhenian area, extensional tectonics affected the Apennines. The intricate tectonic history resulted in a complex system of interconnected faults, which are often activated almost simultaneously, producing close sequences of earthquakes of comparable energy, and frequently with no evidence of primary surface rupture, making the association with any seismogenic source problematic. Clear examples of these effects are the 1997–1998 Umbria-Marche, central Italy sequence (Pino and Mazza, 2000; De Martini *et al.*, 2003) and the 2002 Molise, southern Italy sequence (Di Luccio *et al.*, 2005; Vallée and Di Luccio, 2005).

Considering the devastating effects of previous moderate sequences in Italy, a rapid determination of the source characteristics is particularly important for monitoring the evolution scenarios of the sequence in the perspective of a better hazard assessment. At the Istituto Nazionale di Geofisica e Vulcanologia (INGV) the routinely real or quasi real time analysis, such as earthquake location and magnitude, the estimation of the ground motion shaking and fast moment tensor determinations, does not provide any information about the source characteristics as fault plane discrimination and rupture propagation. With this in mind, we performed a simple waveform analysis right after the April 6, 2009 mainshock in order to investigate the source properties, for a later constraint analysis and for disaster relief. The same investigation was done on the stronger aftershock that occurred on April 7, 2009. A recent paper by Pino and Di Luccio (2009) contains a very brief description of the analysis; in this paper, we illustrate the details of the techniques used.

## 2. Moment rate and direction of rupture propagation

Moderate magnitude earthquakes may evidence important directivity effects that cause strong asymmetry of the radiated energy and, in turn, of the damage distribution. The knowledge of the fracture length and direcrion of propagation greatly helps in determining the areas of stress accumulation caused by the earthquake and, thus, the locus of possible occurrence of impending aftershocks and/or activation of nearby faults, possibly causing similar or even larger events. In fact, as demonstrated in a recent paper by Boatwright (2007), the aftershock distribution is concentrated in the mainshock rupture direction, and this is also verified for moderate earthquakes (*M* = 3.5–4.1). Imaging the rupture extent, especially in areas where potential seismogenic structures are mapped, could help in developing possible scenarios of sequence evolution. Thus, the fast definition of the actual fault plane and its kinematics appears fundamental.

In order to have a fast overview of the energy distribution, for the seismic stations of the INGV National Seismic Network, we plotted the distribution of the local magnitudes $M_L$ for the April 6
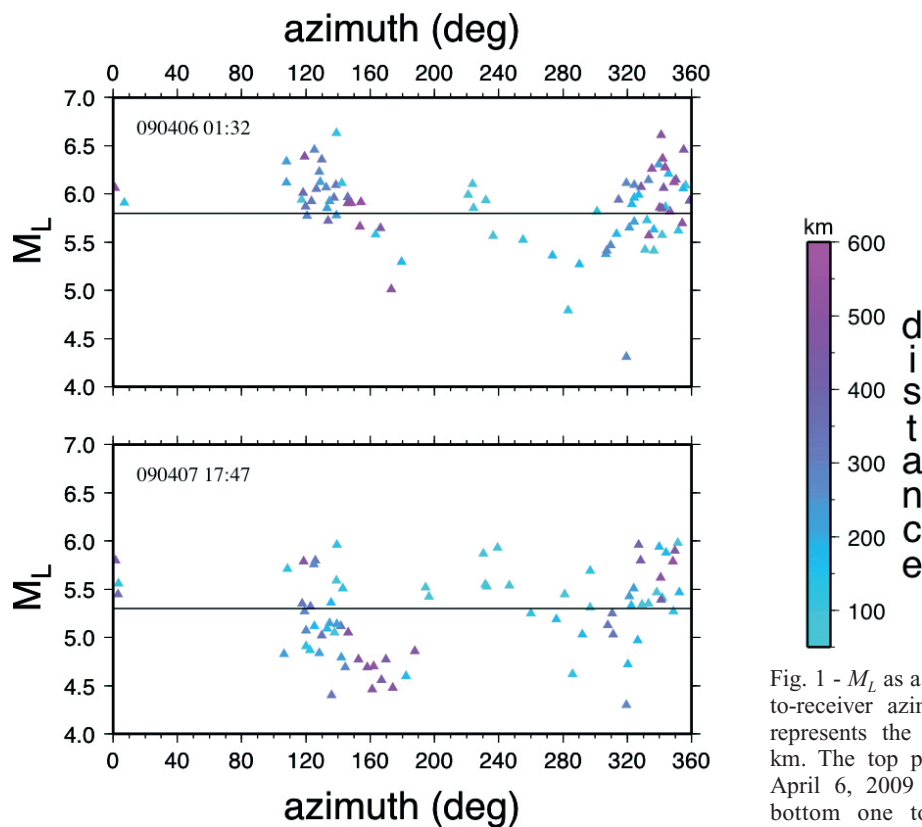
Fig. 1 - $M_L$ as a function of the source-to-receiver azimuth. The color scale represents the epicentral distance in km. The top panel is relative to the April 6, 2009 mainshock, while the bottom one to the April 7, 2009 aftershock.

mainshock against the source-to-station azimuths. Once the waveforms reach the monitoring room, the $M_L$, at each recording station, is available in real time. To identify potential directivity effects, we plotted the local magnitude $M_L$ as a function of the azimuth, taking into account the source-to-station distance (Fig. 1). Distances shorter than 50 km are not considered because the waveforms are saturated. At first, we plotted magnitudes, with respect to the epicenter, averaged in 30° azimuth bins. The resulting picture was not clear enough to give any information. Thus, we preferred to plot each single data point, also considering the source-to-station distance (Fig. 1, top panel). The figure shows overall, clear positive discrepancies between the station estimation and the assigned $M_L$ SE of the mainshock, whereas NW of the mainshock, the negative discrepancies are almost randomly distributed. However, magnitude estimated at stations located between 200 and 300 km from the source give a better defined picture, almost with no values lower than average $M_L$ in the SE sector and very few values higher than the average at NW. A single point at NW displays a very low $M_L$, probably due to a local effect. At longer distances a more confused pattern is displayed. To have a different, and eventually useful view of the local magnitude, we plotted the difference between the station estimate (circle) and the earthquake $M_L$ assigned ($M_L = 5.8$). In Fig. 2a, clear negative discrepancies are displayed NW of the mainshock, whereas, as already observed in Fig. 1, higher magnitudes than the one assigned are found SE of the mainshock.

Table 1 - Source parameters for the mainshock, the 090407 aftershock and the events used as empirical Green function EGF.

| Date (UTC) | Lat. (deg) | Long. (deg) | Depth (km) | $M_L$ | $M_W^1$ | $M_o^1$ (dyne · cm) | Best double couple[1] strike dip rake (deg) | $M_W^2$ | $M_o^2$ (dyne*cm) | Best double couple[2] strike dip rake (deg) |
|---|---|---|---|---|---|---|---|---|---|---|
| 090406 01:32* | 42.35 | 13.4 | 9.5 | 5.8 | 6.1 | $3.7e10^{25}$ | 147 43 -88 /324 47 -92 | 6.3 | $1.8e10^{25}$ | 39 48 -77 /301 43 -104 |
| 090406 03:56 | 42.36 | 13.4 | 10 | 3.9 | - | - | - | 4.3 | $3.5e10^{22}$ | 143 49 -86 /317 41 94 |
| 090407 17:47 | 42.27 | 13.5 | 13.8 | 5.3 | 5.4 | $2.9e10^{24}$ | 336 50 -55 /109 51 -124 | 5.4 | $1.4e10^{24}$ | 338 73 -58 /93 36 -151 |
| 090409 03:14 | 42.36 | 13.5 | 13.7 | 4.2 | 4.4 | $4.9e10^{22}$ | 326 66 -29 /69 63 152 | 4.2 | $2.5e10^{22}$ | 156 87 60 /62 30 175 |

\* The location of the mainshock is from the INGV web site (http://www.ingv.it)
[1] refers to the Quick Centroid Moment Tensor (QCMT, http://earthquake.rm.ingv.it/qrcmt.php)
[2] refers to the INGV Time Domain Moment Tensor (TDMT, http://earthquake.rm.ingv.it/tdmt.php)

Considering the magnitude distribution and the focal solution (Table 1, inset in Fig. 2a), which shows a NW-SE orientation of the two possible planes, the rupture could have propagated in this direction. To quickly verify this hypothesis, we considered a couple of stations (VLC and CUC) located along the fault strike direction, at the same distance from the epicenter but at opposite azimuths (Fig. 2a and Table 2), and computed the relative source time function (RSTF) by frequency domain deconvolution of an empirical Green's function (EGF), with application of a water-level to the spectra. We first chose the aftershock to be used as EGF considering that its focal mechanism and the one of the mainshock have to be the same. The magnitude of the EGF has to be small enough for its source to be considered a delta function, in space and time, but also large enough to be recorded with a good signal-to-noise ratio at all the relevant stations. We restricted our choice to events with location and focal mechanism as close as possible to the large ones. In principle, the nearer the EGF is to the mainshock, the larger the frequency resolved by the method (Patton, 1980); at short periods, depth changes as small as 1 km can affect the estimation of the relative moment rate function. In order to check the similarity of the focal mechanisms between the mainshock and the EGF, we compared the filtered waveforms.

We selected as EGF the aftershock that occurred on April 6, at 03:56 UTC, $M_L = 3.9$, approximately in the same location, with a similar focal mechanism (Table 1 and Figs. 3a and 3b). In general, the frequency resolution of the results depends on the EGF corner frequency (about 1 Hz in this case). We did not filter the waveforms before the deconvolution nor the resulting

Table 2 - Epicentral distance and azimuth of the stations used for the mainshock EGF analysis.

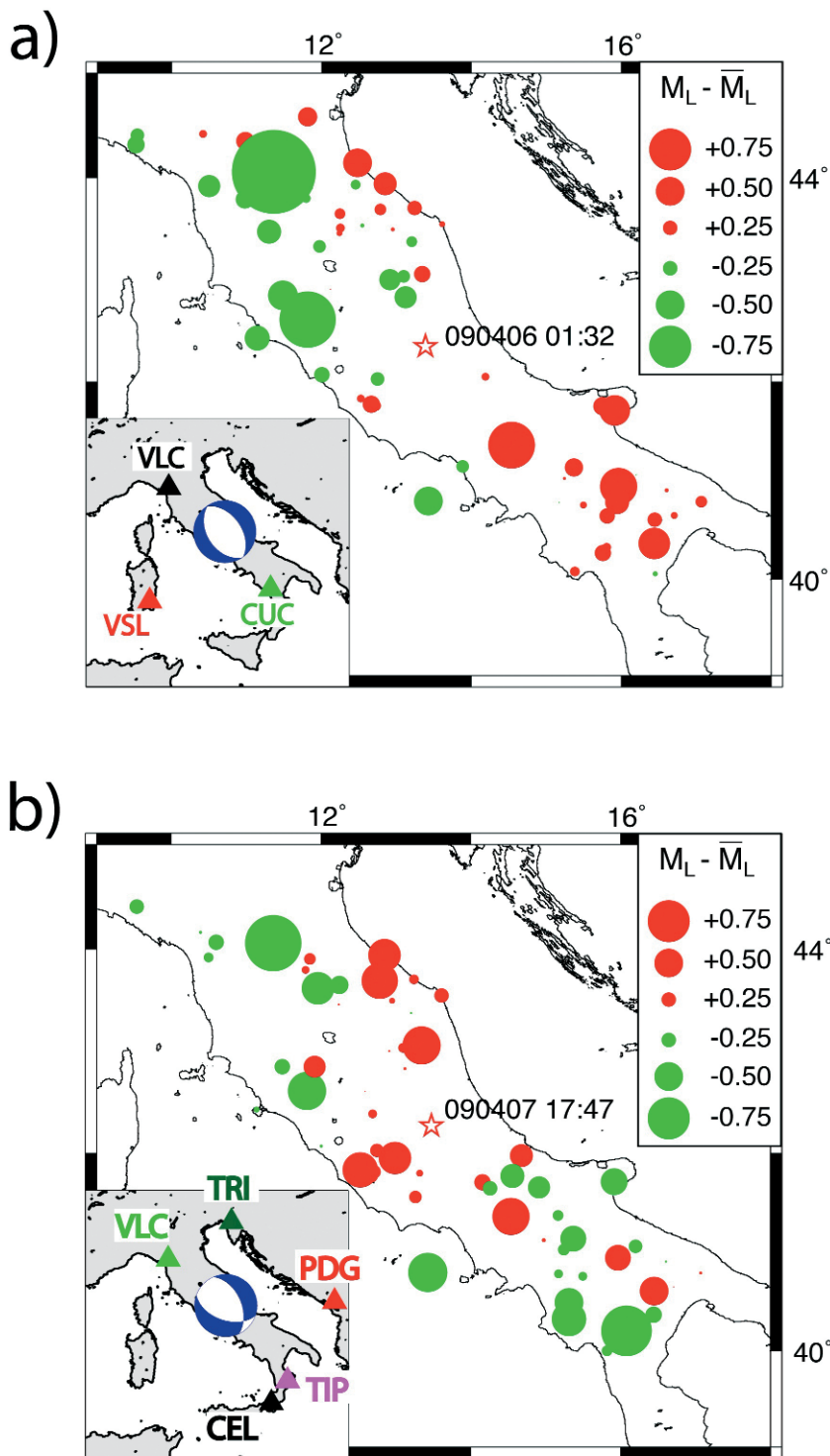| Date (UTC) | CUC dist(km)/az(deg) | VLC dist(km)/az(deg) | VSL dist(km)/az(deg) |
|---|---|---|---|
| 090406 01:32 | 332/141 | 315/311 | 463/228 |
| 090406 03:56 | 332/142 | 316/310 | 465/228 |

Fig. 2 - $M_L$ as computed at the available seismic stations for the mainshock (a) and for the April 7 aftershock, with $\overline{M}_L$= 5.3 (b). Red (green) circles indicate station $M_L$ higher (lower) than the earthquake assigned $\overline{M}_L$ = 5.8. The circle radius is proportional to the magnitude difference; maximum and minimum magnitudo values are 6.63 and 4.31, respectively. In the bottom right inset the Quick Regional Centroid Moment Tensor (QRCMT, http://mednet.rm.ingv.it/quick_rcmt. php) along with the station locations are displayed.

a)

main:   090406 01:32
EGF:    090406 03:56

c)

main:   090407 17:47
EGF:    090409 03:14

Station PDG - band passed 0.005-0.08 Hz

Station PDG - band passed 0.005-0.08 Hz

b)

090406 01:32      090406 03:56

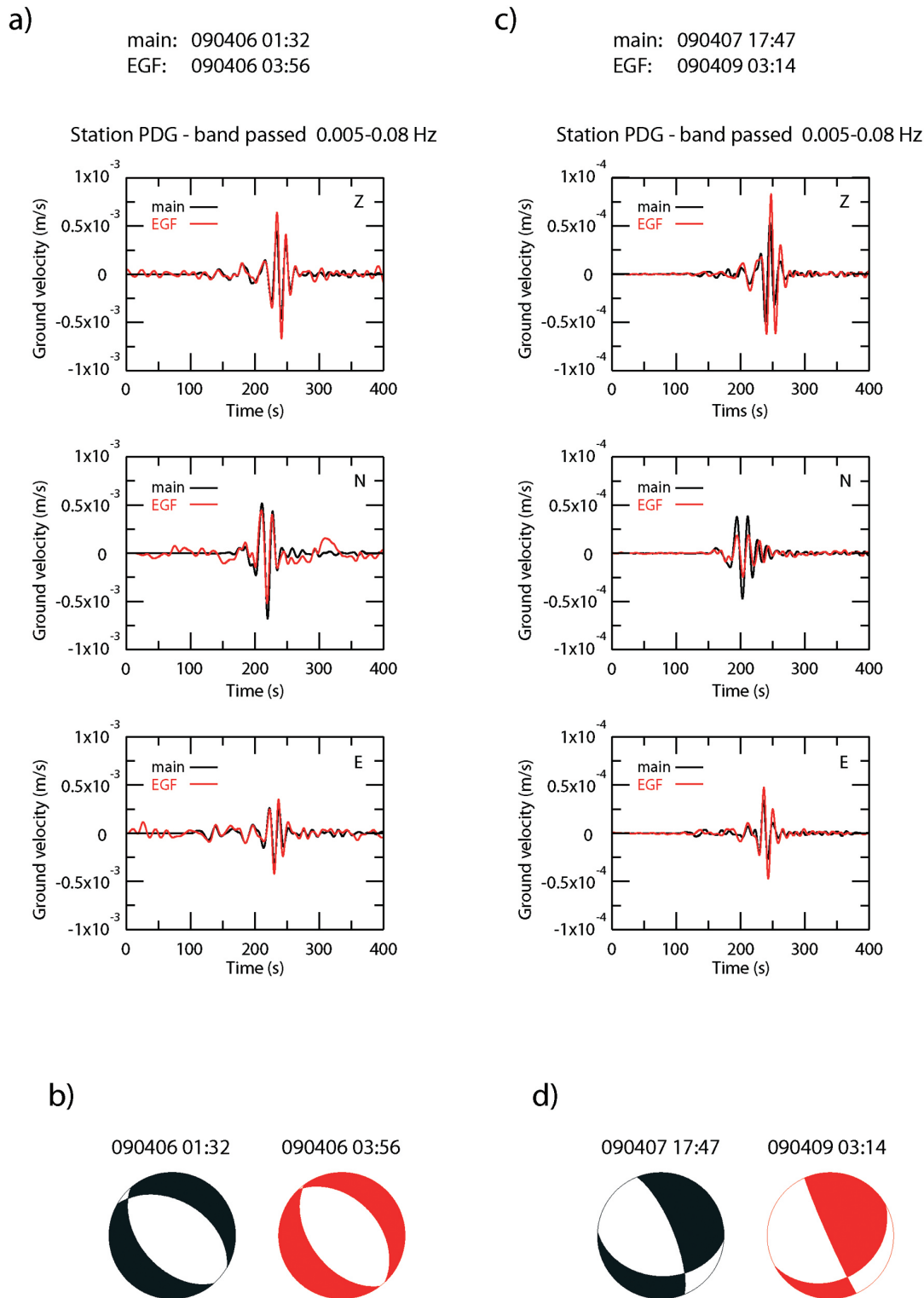d)

090407 17:47      090409 03:14

Fig. 3 - Comparison between the filtered waveforms relative to the mainshock and the chosen EGF for the 090406 01:32 event (a) and analogous comparisons for 090407 17:47 event (c). b) and d) QRCMTs for the mainshock (b), the April 7 aftershock and its EGF (d), while the TDMT solution is plotted for the 090406's EGF mechanism.
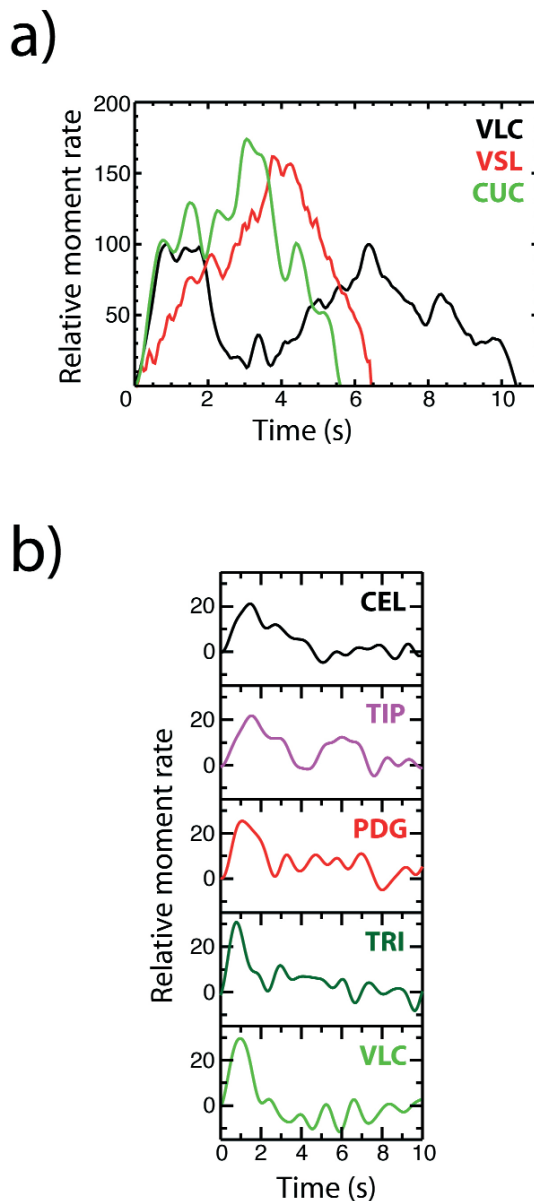
a)



b)



Fig. 4 - Unfiltered RSTFs for the mainshock (a), resulting at the selected stations (shown in Fig. 2a inset) and for the aftershock (b), resulting at the selected stations (Fig. 2b inset).

RSTFs. At the considered epicentral distances, the far-field approximation can be well considered valid for the chosen aftershock, thus the EGF source can be assumed point-like. The RSTF resulting at VLC, displays a significantly longer duration and lower maximum amplitude with respect to the one obtained at CUC (Fig. 4a), clearly confirming the net SE-ward propagation of the rupture. The two RSTFs have very similar shapes during the first 2 seconds. This feature can be explained either by a bilateral, along-strike (possibly circular) rupture or by fracture propagation perpendicular to the path of each of the two stations, i.e., perpendicular to the fault strike. To solve this ambiguity, we computed the RSTF at VSL, located at about 90° from the fault strike (Fig. 2a, bottom left inset). The smaller amplitude resulting for the first pulse at this station with respect to VLC and CUC implies that the fracture initially propagated in a direction opposite to the path of the VSL. Incidentally, we noticed that the three RSTFs give very similar relative seismic moments (all around 490) that, when multiplied by the seismic moment of the EGF, are in agreement with the $M_0$ resulting from waveform inversion for moment tensor determination (Table 1). Thus, the mainshock occurred in two distinct sub-events, a first one with fracture propagating NE-wards from the hypocenter, followed by a second rupture patch located SE of the previous one. Due to the similarity between the strike of the conjugated planes, the directivity analysis does not allow the discrimination of the fault responsible for this earthquake. However, by neglecting the differences between the two sub-events of the rupture process and assuming the actual rupture duration as the mean between the result at VLC and CUC, an indicative fault length of about 20 km is inferred for a fracture velocity of 2.5 km/s.

Table 3 - Epicentral distance and azimuth of the stations used for the 090407 aftershock EGF analysis.

| Date (UTC) | CEL dist(km)/az(deg) | PGD dist(km)/az(deg) | TIP dist(km)/az(deg) | TRI dist(km)/az(deg) | VLC dist(km)/az(deg) |
|---|---|---|---|---|---|
| 090407 17:47 | 491/154 | 477/86 | 441/140 | 383/3 | 327/311 |
| 090409 03:14 | 500/155 | 478/87 | 450/141 | 373/364 | 320/310 |

These results fully confirm what was suggested by the magnitude distribution (Figs. 1 and 2), indicating that helpful information on the source directivity can be quickly derived from a simple plot that, in turn, can be easily obtained in real time analyses.

The above investigation is then done for the strongest aftershock. In Fig. 1, bottom panel, the magnitude distribution with azimuth seems to put in evidence the presence of negative anomalies SE of the event and more sparsely positive discrepancies towards north. Again stations between 200 and 300 km define a better picture, with a relatively large negative anomaly displayed at the same station that gives the very low magnitude for the mainshock. This evidence confirms that at this particular site $M_L$ is significantly underestimated. The same general pattern is observed in Fig. 2b, where the difference between the local magnitude at each station and the $M_L$ assigned for the April 7 aftershock, displays a more confused pattern, with respect to the mainshock, although some indication of larger magnitudes north of the epicenter is put in evidence. We computed RSTFs for this strong aftershock. Due to the difference between the strike orientation of the conjugated planes (Fig. 2b and Table 1) and the relatively small magnitude, we analyzed a few stations, rather than just a couple, covering a large azimuth range (Fig. 2b and Table 3). By choosing the aftershock that occurred on April 9, at 03:14 UTC, $M_L = 4.2$ (Table 1 and Figs. 3c and 3d) as EGF, we obtained durations ranging from 2 s to 5 s (Fig. 4b). Due to the higher noise level, with respect to the mainshock, we low-pass filtered the resulting functions at 1 Hz. Similarly to the mainshock, in the analyzed distance and frequency range, the EGF can be considered a point-source event. The relative seismic moments are all in the range 40–50, giving a good agreement with the absolute $M_0$. The RSTFs exhibit a clear pattern with longer apparent durations and lower amplitudes toward S–SE, while the shortest durations are displayed at VLC and TRI, their azimuths relative to the epicenter are 311° and 350°, respectively. According to its focal mechanism, the rupture associated to the April 7 aftershock could have interested either the approximately EW-oriented fault plane, with updip propagation, or the N-NW-oriented fault plane, with horizontal propagation.

## 3. Fault plane discrimination

The directivity analysis does not help in the discrimination of the fault plane for both the mainshock and its stronger aftershock, however the surface deformation for one plane or the conjugate is expected to be different. Thus, we used the waveforms from the available strong motion stations distributed in the epicentral area to image the surface deformation, estimating the static vertical deformation. In particular, we analyzed data recorded at the MedNet accelerometer installed at L'Aquila (AQU) and the accelerometers of the National Accelerometric Network, run

by the Italian Civil Protection (http://www.protezionecivile.it), close to the epicenter.

Permanent displacements produced by an earthquake are the zero-frequency part of the seismic signal. They provide information about the size and final slip distribution of the earthquake source and are not sensitive to details of the source rupture process and of the Earth structure. Starting from acceleration waveforms, integrating twice we obtain displacement. Due to the integration process, the resulting signal contains a drift that needs to be removed to get the static displacement. The correction for the baseline drift in the displacement waveform after removing instrument response is a crucial point. Recently, Zhu (2003) proposed a technique to recover the ground displacement from broadband seismic recordings, which proved to be very effective. This technique already produced reliable results for the largest events in the 2002 Molise (southern Italy) sequence ($M_W = 5.7$–5.8), allowing the estimate of static displacement to be as small as a few tenths of a millimeter, at 50 km from the epicenter (Pino and Di Luccio, 2005). In particular, Zhu (2003) proposed a time-domain algorithm to remove instrument response and to restore baselines. A nice feature of the algorithm is that it gives the optimal estimation of a permanent offset, which is determined by a least-square inversion in the drift correction procedure. The traditional methods of frequency-domain deconvolution and filtering tend, instead, to destroy the pre- and after-signal baselines. Following Zhu (2003), we assume that the ground is at rest initially, then a time domain recursive filter can be derived to compute the ground velocity $v_i$:

$$v_i = 2v_{i-1} - v_{i-2} + \frac{1}{G}(az_i + bz_{i-1} + z_{i-2}),$$

$$v_0 = 0$$

$$v_1 = 0, \quad where$$

$$a = 1 + 2h\omega_0\Delta t + \omega_0^2\Delta t^2$$

$$b = -2(1 + h\omega_0\Delta t)$$

and $\Delta t$ is the sampling interval. By integrating $v_i$, raw ground displacements can be calculated. Unlike frequency domain deconvolution, which usually involves band-pass filtering of data to stabilize the operation, the above algorithm does not alter the long-period content of the signal. This produces only a negligible difference up to 1 Hz with respect to the exact response, but ensures stable signals.

Applying this procedure, we obtained ground displacement waveforms from the original acceleration recordings by double integration. The resulting waveforms display a large drift that makes the estimate of the permanent displacement very problematic and even masks earthquake signals. Fig. 5 shows an example of the displacement vertical component at one of the recording stations, where the raw displacement clearly shows the effect of drift. Again, following Zhu (2003), we assumed that drift is a smoothly varying function that can be modeled by a low-order polynomial:
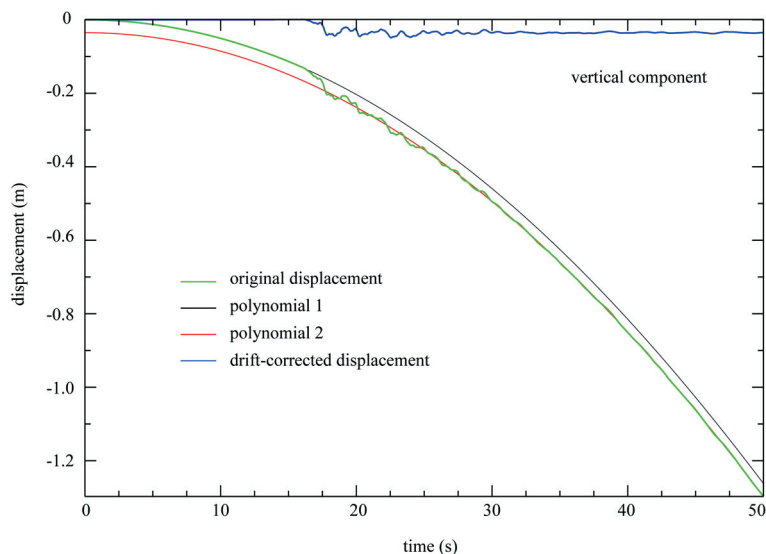
$$p(t) = \sum_{i=0,n} c_i t^i$$

Fig. 5 - Example of displacement waveform for the April 6, 2009 mainshock.

If the transient signal produced by the earthquake lasts from time $t_1$ to $t_2$ at the site, the following equations can be established:

$$c_0 + c_1 t + ... + c_n t^n = u(t) \qquad\qquad t < t_1;$$
$$\delta + c_0 + c_1 t + ... + c_n t^n = u(t) \qquad\qquad t > t_2;$$

where the constant term $\delta$ is the static displacement. The above is a linear equation system about $c_i$'s and $\delta$ and the best fitting coefficient are searched by a least-square inversion. Corrected displacement waveform is obtained by subtracting the polynomial $p(t)$ from the deconvolved displacement $u(t)$. The procedure eliminates the need to measure the permanent displacement on the corrected displacement waveform because $d$ is determined as part of the least-square inversion. By using a 4th-order polynomial for both events we obtained the waveforms displayed in Fig. 6.

We also searched for further constraints by evaluating the tilt affecting the seismic recordings. In principle, a seismic sensor responds to acceleration changes occurring along its sensitive axis. Ground tilt, which causes relative displacement of the sensitive mass with respect to the reference frame, could be well recorded by a seismic instrument and, usually, with larger amplitude on the horizontal components, more sensitive to sensor tilting (see, e.g., Pillet and Virieux, 2007). The result strongly depends on the precision of the sensor vertical alignment, thus we only analyzed data from the MedNet accelerometer installed at the AQU site, being more reliable as quality of installation. In Fig. 7, the filtered acceleration time history for the three components of the mainshock and its stronger aftershock are shown, along with the their relative particle motion. The ground tilt component is evident mostly on the horizontal components of the signals.

Fig. 8a shows the results for the mainshock at the available accelerometers, indicated in the
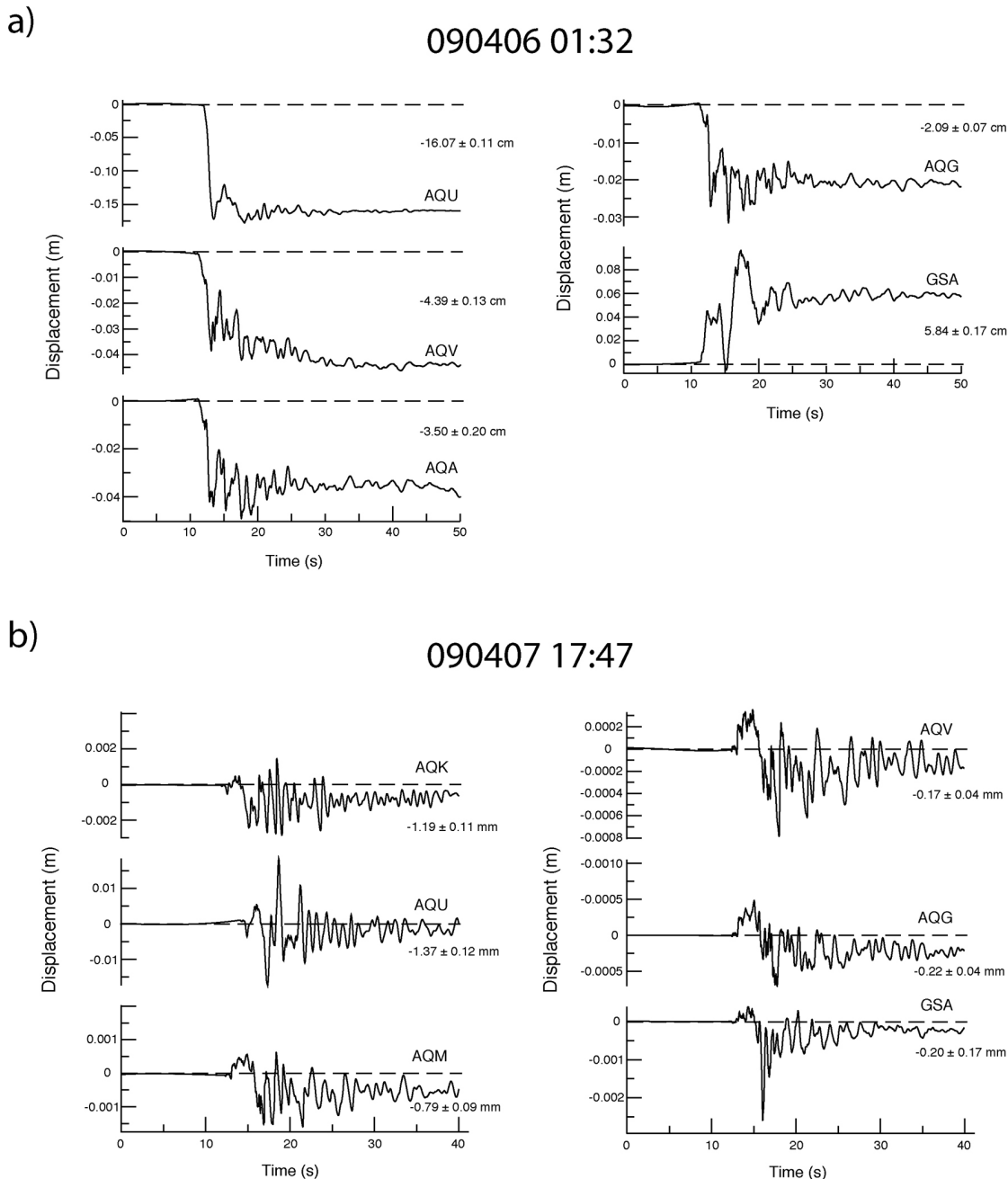
a)

## 090406 01:32



b)

## 090407 17:47



Fig. 6 - Corrected displacement waveforms with the estimated static offset, derived from accelerometric recordings at the indicated stations for the 090406 01:32 and 090407 17:47 events.

figure's right panel, together with the surface deformation predicted for simple model faults corresponding to each of the conjugated planes. Stations with clipped signals are not considered. We assumed a 17 x 12 km$^2$ plane, whose top was located at a depth of 1.5 km, and a uniform slip of 62 cm.
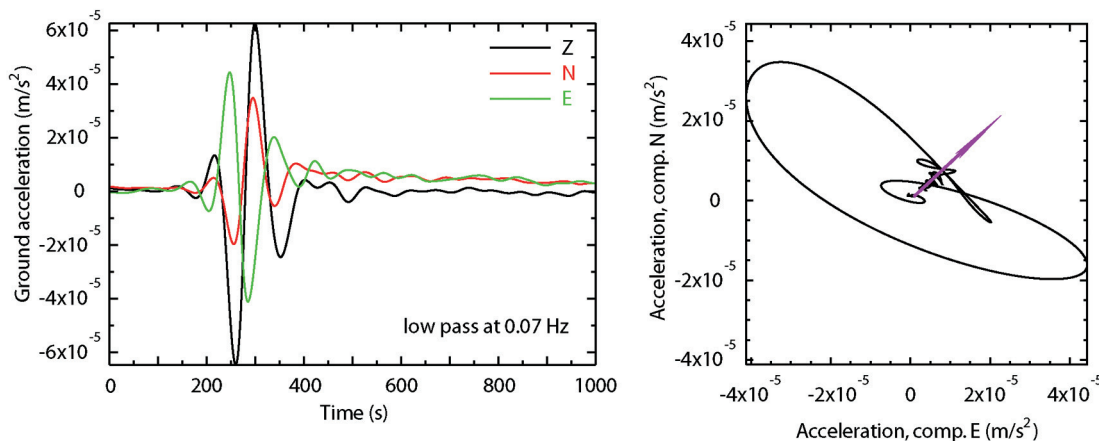
a)

## 090406 01:32
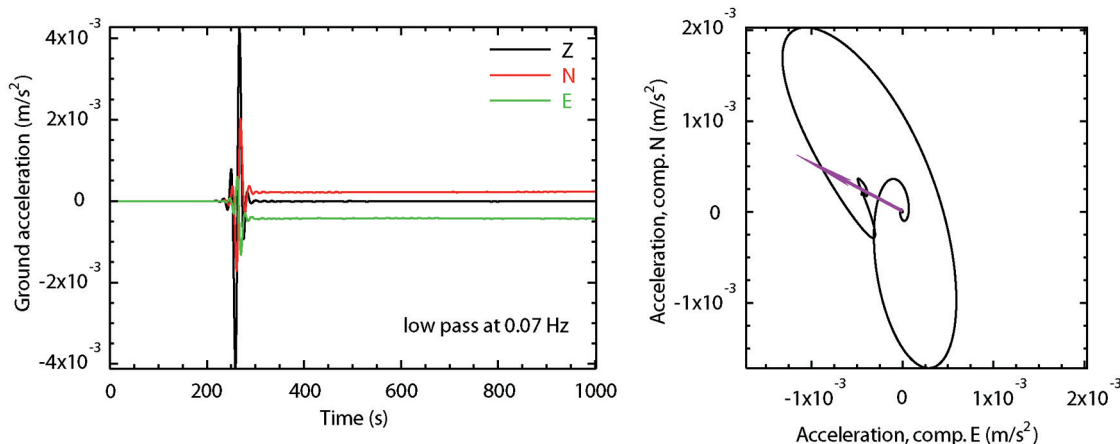


b)

## 090407 17:47



Fig. 7 - Filtered acceleration time history on the three components for the 090406 01:32 and 090407 17:47 events.

Apparently, the SW-dipping plane (Fig. 8a, left) gives a much better fit to the vertical displacement data with respect to the other plane (Fig. 8a, right) and, in spite of only a single measurement, the deformation gradient is convincingly parallel to the observed tilt direction. This evidence strongly supports the SW-dipping fault as responsible for the earthquake, as also confirmed by the InSAR data analysis (Atzori *et al*., 2009). According to this conclusion, the first
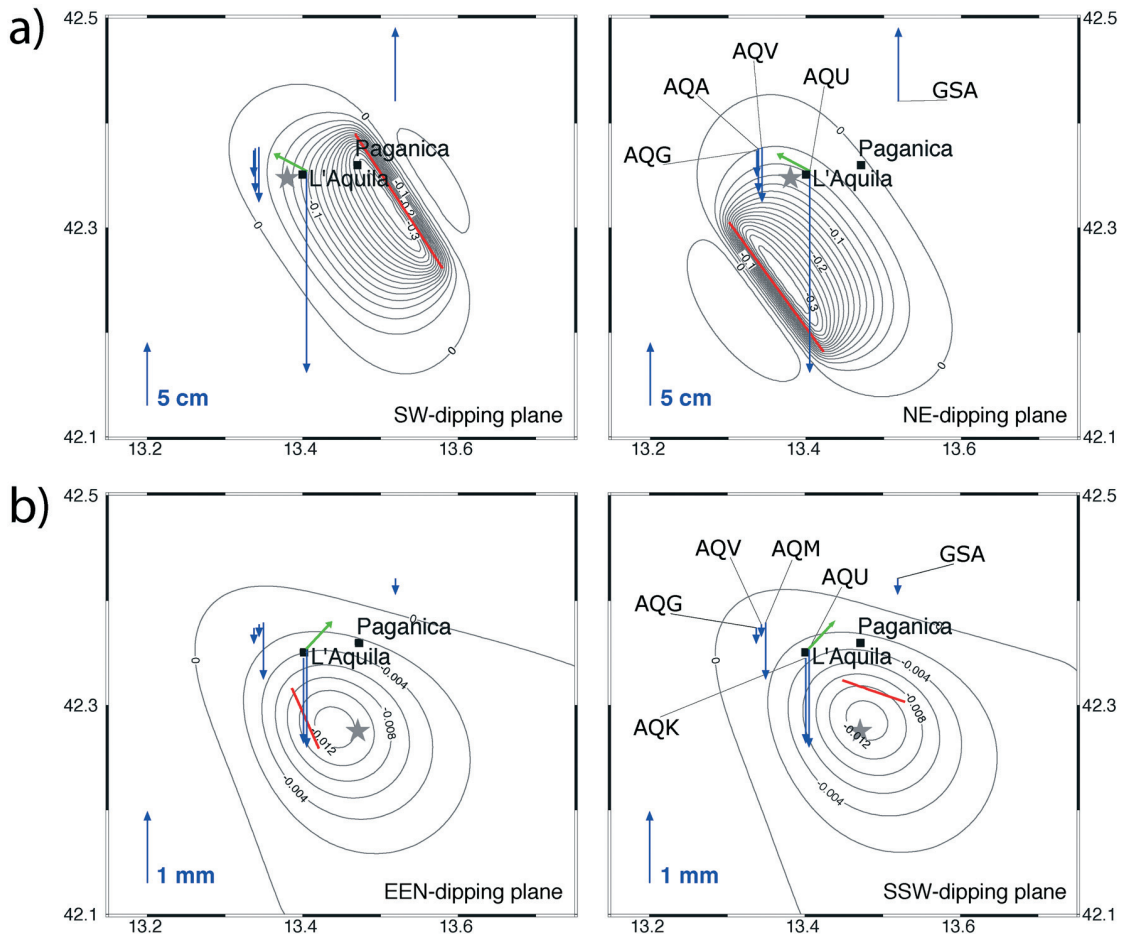
Fig. 8 - a) Comparison between the vertical static deformation (blue arrows), measured at the available broadband station (AQU) and accelerometers, along with the tilt direction estimated at the AQU accelerometer (green arrows), and the theoretical surface deformation (grey lines; unit in cm) predicted for the mainshock (a) and for the April 7 aftershock (b) by imposing uniform slip on each of the two conjugated planes, in a homogeneous halfspace. The red line and the star mark the fault surface projection and the epicenter, respectively. In both cases, we used the program EDCMP (Wang *et al*., 2003) to compute theoretical surface deformation.

rupture stage occurred with updip fracture propagation.

## 3. Slip distribution

We followed Kanamori *et al*. (1992) and converted the RSTF to a slip distribution along the fault strike, both for the mainshock and the April 7 aftershock. This approach assumes a unilateral fracture propagation, thus, for the April 6 event, we first split the RSTF resulting at VLC (Fig. 4a) into two pieces, from 0 s to 3 s and from 3 s to 10.4 s, associated with moment released respectively by the updip and the horizontal rupture propagation, obtaining two separate moment rate functions, each one corresponding to a single segment of unilateral rupture propagation. The

function resulting for the second stage represents the apparent moment rate $\dot{M}$, as observed at 180° with respect to the propagation direction, but needs to be scaled to the appropriate amplitude and duration to get the actual $\dot{M}$. Then, we merged the two functions, by assuming a horizontal length of about 3 km for the first rupture. The along-strike slip distribution defines a fault length of 17–18 km, with major dislocation peaks of about 0.8 m and 1.2 m at 0 km and 9 km, respectively, a strongly reduced slip in between, and a distinct relative maximum at about 13 km (Fig. 9a). The updip rupture propagation, provides a reasonable, at least partial, explanation for the strong damage observed at several localities close to the top of the fault sector ruptured during the first stage. At the AQU accelerometer, a peak ground acceleration in excess of 0.3 g and 0.16 cm subsidence results from our analysis.

Although representing a first approximation, our conclusions are in excellent agreement with the results of joint inversion of GPS and strong motion data performed successively by Cirella *et al*. (2009). We point out that our results do not depend on a specific starting assumption and so they can be used as evaluation of independent inversions.

The rupture pattern clearly delineates two separate patches, with the first located in proximity of Paganica, where the aftershock distribution defines a distinct fault plane [Fig. 9c and Di Luccio *et al*. (2010)] and evidence of surface fracture was detected during field surveys (EMERGEO Working Group, 2009); the other one occurring further SE, where the aftershock epicenters are roughly aligned along a N-S direction, deviating from the fault strike, and apparently the hypocenters do not define the same fault surface (Fig. 9c). Actually, this second slip patch is where the maximum fault dislocation of 1.2 m occurs.

Moreover, the relatively high RSTF amplitude resulting at VSL (90° azimuth relative to the fault strike, Fig. 4a) for this second rupture stage indicates that the fracture could have propagated along a different direction from the fault strike and closer to the path of the VSL. If this is the case, assuming the fault plane as a single plane, the derived rupture is consequently downwards. It is observed that the fracture deepens in the area where the slip is maximum and the main fault plane is no longer clearly identified. This could suggest that the original plane has broken and a new rupture is generated. In general, the second, larger, rupture stage might have occurred on a different plane, activating a separate fault system. In this regard, the conclusions of Atzori *et al*. (2009) and Cirella *et al*. (2009), depicting a slip distribution deepening to the south might be from the assumption of a single fault plane. Since the southernmost event shows a larger strike-slip component, also Pondrelli *et al*. (2010) proposed the involvement of a distinct fault system to the south. More recently, Guerrieri *et al*. (2010) modeled the InSAR data by using two fault segments dipping 45°, with the southern plane at a lower strike angle, and they obtained lower data misfits with respect to a single fault plane. Their preferred geometry is not necessarily the actual one, nevertheless their results further indicate that some discontinuity in the rupture plane is likely to have occurred.

Finally, we remark that the clear separation between the two main rupture patches is likely to have caused the significant difference in the estimates of $M_L$ and $M_W$. We speculate that, in general, at frequencies relevant to $M_L$ evaluation (around 1 Hz), the energy radiated by two relatively distant patches does not interact, while it does at a lower frequency, where the seismic moment, thus $M_W$, is computed.

As expected from its magnitude and hypocentral depth, the surface deformation resulting for
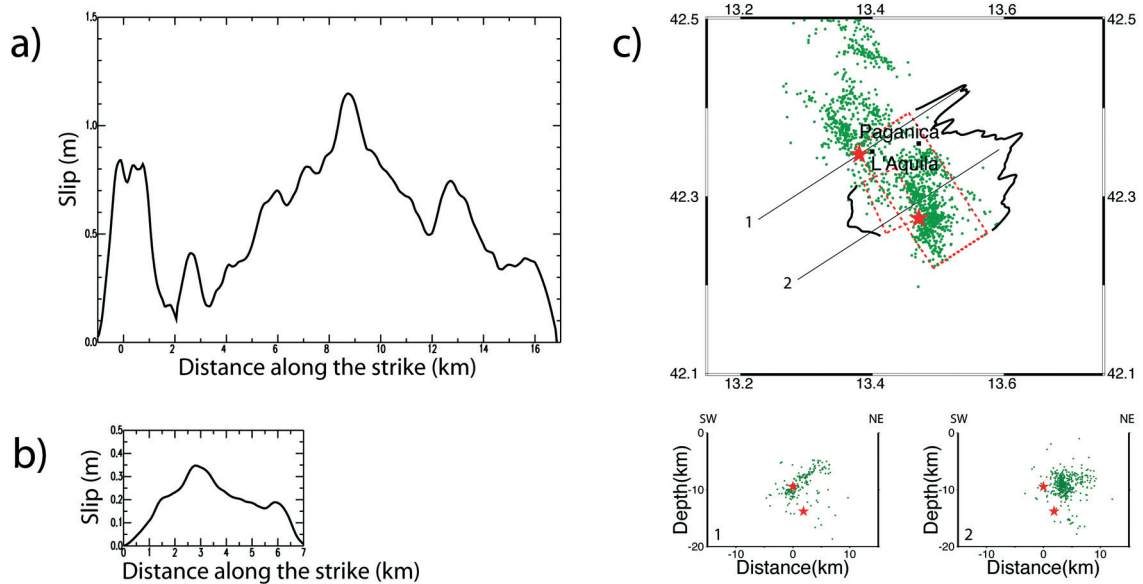
Fig. 9 - a) Along-strike slip distribution for the mainshock, obtained for rupture velocity $v_r$=2.5 km/s, rigidity $\mu$=3 x $10^{10}$ N/m$^2$, and fault width $w$=10 km (a) and for the April 7 aftershock, obtained for rupture velocity $v_r$=2.8 km/s, rigidity $\mu$=3 x $10^{10}$ N/m$^2$, and fault width $w$=7 km (b). The zero distance indicates the epicenter position. Surface projection (red dashed) of the fault planes (c), along with the slip distribution for the studied events (black lines). Aftershock locations (green dots) that occurred until April 30 is reported (Di Luccio *et al*., 2010), with their depth distribution along sections 1 and 2 (width 6 km).

the April 7 event is very small (Fig. 8b), more than one order of magnitude smaller than that observed for the mainshock. For this event, we assumed a uniform slip of 19 cm and a 7 x 7 km$^2$ fault plane, with top edge at a depth of 9.6 km. At the location of the available accelerometric stations (Fig. 8b, right), the difference between the results for the two conjugated planes does not allow the unequivocal discrimination of the rupture surface. Besides, for both model faults, the predicted surface displacement is larger than the observed one. Results do not change if reasonably larger or smaller faults were assumed. A sole indication derives from the tilt observed at AQU, for which the N336° plane (Fig. 8b, left) seems to be slightly preferred. Thus, we favor this latter as actual rupture plane and conclude that the fracture initiated in proximity of its southern end and propagated northwards. Unfortunately, there is no evidence of surface rupture for this event, which is located at a 14 km depth, whereas its related cluster of seismicity is concentrated between a 6 and 12 km depth (Fig. 9c). Likely the focus of the April 7 event is separated from the shallower cluster by an aseismic shearing zone as speculated by Di Luccio *et al*. (2010). Assuming the initiation of several collinear normal faults during the 2009 L'Aquila sequence, Di Luccio *et al*. (2010) hypothesize that the propagation of a fluid pressure wave through an anisotropic fractured rock is the cause of the interaction and activation of these faults.

According to the source duration observed at an azimuth of about 90° from the fault strike, a rupture length of about 6.0–7.0 km results if a fracture velocity of 2.5–3.0 km/s is assumed. Similarly to what we did for the mainshock, we considered the most stable RSTF resulting on the

less directive side (TIP, Fig. 4b) and converted it to slip distribution along the fault strike, obtaining an asymmetrical function with a maximum of about 35 cm, at less than 3 km from the hypocenter, and lower slip, with a maximum of less than 20 cm, toward the far fault end (Fig. 9b). This heterogeneous distribution could be the cause for the discrepancy between the magnitude of the vertical deformation observed at the seismic stations and subsidence predicted for uniform slip fault. At the moment, the present analysis represents the only investigation of the April 7 aftershock and, as for the static surface deformation, we do not expect a more precise investigation from GPS or InSAR data, as they are not sensitive enough.

## 4. Conclusions

As soon as the waveforms of the April 6, 2009 L'Aquila earthquake were available, basic seismic waveform analysis was done in order to derive useful and well-constrained source information. By applying the empirical Green's function approach at selected stations, we could rapidly determine the rupture propagation direction for the mainshock and the major aftershock. The $M_L$ distribution and the vertical, permanent displacement computed for the two events contributed to the discrimination of the fault plane and gave first rough estimates of the slip distribution along the fault planes involved. We found that two distinct rupture patches associated with different fracture propagation directions and possibly occurring on distinct rupture planes, characterized the source kinematics of the April 6 events. Our result was successively confirmed by independent, more sophisticated, analysis, as seismic and surface deformation data.

This fast and elementary seismological analysis requires a very short time. The magnitude $M_L$ evaluated at each single station is available just a few minutes after the earthquake, while, as soon as the waveforms of a suitable aftershock are available, the EGF analysis is almost immediate. Usually, smaller events with similar location and source mechanism occur within tens of minutes to a few hours after the mainshock and, in principle, good EGF's can even be provided by foreshocks [see, for instance, Pino *et al.* (1999)]. EGF analysis does not need any specific assumption and provides useful constraints for more refined investigations, such as complex, massive, inversion of data for imaging the rupture evolution and the slip distribution on the fault plane. As a matter of fact, especially for moderate magnitude events, these latter can be quite unstable and independently derived information greatly helps in constraining the solution.

We suggest that these analyses could be included in a real time analysis system. In fact, simple plots of magnitude distribution, in a geographical map and/or as a function of the source-to-station azimuth, can be easily produced immediately after the quake. On the other hand, effective EGF techniques could be implemented with little computational efforts, for instance, by automatically searching the best event to be used as reliable empirical Green's function, among foreshocks or in early aftershocks that occurred at a close distance to the main event.

## REFERENCES

Atzori S., Hunstad I. , Chini M., Salvi S., Tolomei C., Bignami C., Stramondo S., Trasatti E. and Antonioli A.; 2009: *Finite fault inversion of DInSAR coseismic displacement of the 2009 L'Aquila earthquake (central Italy).* Geophys. Res. Lett., **36**, L15305, doi: 10.1029/2009GL039293.

Boatwright J.; 2007: *The persistence of directivity in small earthquakes.* Bull. Seismol. Soc. Am., **97**, 1850–1861, doi: 10.1785/0120050228.

Cirella A., Piatanesi A., Cocco M., Tinti E., Scognamiglio L., Michelini A., Lomax A. and Boschi E.; 2009: *Rupture history of the 2009 L'Aquila earthquake from non-linear joint inversion of strong motion and GPS data.* Geophys. Res. Lett., **36**, L19304, doi: 10.1029/2009GL039795.

De Martini P.M., Pino N.A., Valensise G. and Mazza S. ; 2003: *Geodetic and seismologic evidence for slip variability along a blind normal fault in the Umbria-Marche 1997–1998 earthquakes (central Italy).* Geophys. J. Int., **155**, 819– 829, doi: 10.1111/j.1365-246X.2003.02049.x.

Di Luccio F., Fukuyama E. and Pino N.A.; 2005: *The 2002 Molise earthquake sequence: What can we learn about the tectonics of southern Italy?* Tectonophysics, **405**, 141-154, doi: 10.1016/j.tecto.2005.05.024.

Di Luccio F., Ventura G., Di Giovambattista R., Piscini A. and Cinti F.R.; 2010: *Normal faults and thrusts re-activated by deep fluids: the 6 April 2009 $M_W$ 6.3 L'Aquila earthquake, central Italy.* J. Geophys. Res., **115**, B06315, doi: 10.1029/2009JB007190.

Doglioni C.; 1991: *A proposal of kinematic modelling for W-dipping subductions – Possible applications to the Tyrrhenian - Apennines system.* Terra Nova, **3**, 423-434.

EMERGEO Working Group; 2010: *Evidence for surface rupture associated with the $M_W$ 6.3 L'Aquila earthquake sequence of April 2009 (central Italy).* Terra Nova, **22**, 43-51, doi: 10.1111/j.1365-3121.2009.00915.x.

Guerrieri L., Baer G., Hamiel Y., Amit R., Blumetti A.M., Comerci V., Di Manna P., Michetti A.M., Salamon A., Mushkin A., Sileo G. and Vittori E.; 2010: *InSAR data as a field guide for mapping minor earthquake surface ruptures: ground displacements along the Paganica Fault during the April 6th, 2009, L'Aquila earthquake.* J. Geophys. Res., **115**, B12331, doi: 10.1029/2010JB007579.

Kanamori H., Thio H., Dreger D., Hauksson E. and Heaton T.; 1992: *Initial investigation of the Landers, California, earthquake of 28 June 1992 using TERRAscope.* Geophys. Res. Lett., **19**, 2267–2270, doi: 10.1029/92GL02320.

Patacca E., Sartori R. and Scandone P.; 1992: *Tyrrhenian basin and Apenninic arcs: Kinematics relations since Late Tortonian times.* Mem. Soc. Geol. It., **45**, 425-451.

Patton H.; 1980: *Reference point equalization method for determining the source and path effects of surface waves.* J. Geophys. Res., **85**, 821-848.

Pillet R. and Virieux J.; 2007: *The effects of seismic rotations on inertial sensors.* Geophys. J. Int., **171**, 1314–1323, doi: 10.1111/j.1365-246X.2007.03617.x.

Pino N.A. and Di Luccio F.; 2005: S*eismic recording of small zero frequency displacement from moderate events.* Geophys. Res. Lett., **32**, L12304, doi: 10.1029/2005GL022780.

Pino N.A. and Di Luccio F.; 2009: *Source complexity of the 6 April 2009 L'Aquila (central Italy) earthquake and its strongest aftershock revealed by elementary seismological analysis.* Geophys. Res. Lett., **36**, L23305, doi: 10.1029/2009GL041331.

Pino N.A. and Mazza S.; 2000: *The Umbria-Marche (central Italy) earthquakes: Relation between rupture directivity and sequence evolution for the $M_W$ > 5 shocks.* J. Seismol., **4**, 451-461, doi: 10.1023/A:1026579300852.

Pino N.A., Mazza S. and Boschi E.; 1999: *Rupture directivity of the major shocks in the 1997 Umbria-Marche (Central Italy) sequence from regional broadband waveforms.* Geophys. Res. Lett., **26**, 2101-2104.

Pondrelli S., Salimbeni S., Morelli A., Ekström G., Olivieri M. and Boschi E.; 2010: *Seismic moment tensors of the April 2009, L'Aquila (central Italy), earthquake sequence.* Geophys. J. Int., **180**, 238-242, doi: 10.1111/j.1365-246X.2009.04418.x.

Vallée M. and Di Luccio F.; 2005: *Source analysis of the 2002 Molise, southern Italy, twin earthquakes (10/31 and 11/01).* Geophys. Res. Lett., **32**, L12309, doi: 10.1029/2005GL022687.

Wang R., Lorenzo-Martín F. and Roth F.; 2003: *Computation of deformation induced by earthquakes in a multi-layered elastic crust—FORTRAN programs EDGRN/EDCMP.* Comput. Geosci., **29**, 195–207, doi: 10.1016/S0098-3004(02)00111-5.

Wessel P. and Smith W.H.F.; 1991: *Free software helps map and display data.* Eos Trans. AGU, **72**, 441, doi:

10.1029/90EO00319.

Zhu L.; 2003: *Recovering permanent displacements from seismic records of the June 9, 1994 Bolivia deep earthquake.* Geophys. Res. Lett., **30**, 1740, doi: 10.1029/2003GL017302.

*Corresponding author:*   Nicola Alessandro Pino
                          Istituto Nazionale di Geofisica e Vulcanologia, Osservatorio Vesuviano
                          Via Diocleziano 328, 80124 Napoli, Italy
                          Phone: +39 081 6108545; fax: +39 081 6108351; e-mail: alessandro.pino@ov.ingv.it.